Modeling charged defects, dopant diffusion and activation mechanisms for TCAD simulations using Kinetic Monte Carlo

Ignacio Martin-Bragado, S. Tian and M. Johnson

Synopsys Inc, 700 East Middlefield Road, Mountain View, 94043 CA USA

P. Castrillo, R. Pinacho, J. Rubio and M. Jaraiz.

Dept. of Electronics. University of Valladolid

Campus Miguel Delibes, Camino del Cementerio S/N. 47011

Valladolid, Spain.

This work will show how the Kinetic Monte Carlo (KMC) technique is able to successfully model the defects and diffusion of dopants in Si-based materials for advanced microelectronic devices, especially for non-equilibrium conditions. Charge states of point defects and paired dopants are also simulated, including the dependency of the diffusivities on the Fermi level and charged particle drift coming from the electric field.

The KMC method is used to simulate the diffusion of the point defects, and formation and dissolution of extended defects, whereas a quasi-atomistic approach is used to take into account the carrier densities. The simulated mechanisms include the kick-out diffusion mechanism, extended defect formation and the activation/deactivation of dopants through the formation of impurity clusters. Damage accumulation and amorphization are also taken into account. Solid Phase Epitaxy Regrowth is included, and also the dopants redistribution during recrystallization of the amorphized regions.

Regarding the charged defects, the model considers the dependencies of charge reactions, electric bias, pairing and break-up reactions according to the local Fermi level. Some aspects of the basic

physical mechanisms have also been taken into consideration: how to smooth out the atomistic dopant point charge distribution, avoiding very abrupt and unphysical charge profiles, how to correctly and effectively update the charge, and how to implement the drift of charged particles into the existing electric field.

The work will also discuss the efficiency, accuracy and relevance of the method, together with its implementation in a Technology Computer Aided Design process simulator.

1. Introduction

The trend of reducing device sizes results in a small number of impurity atoms that determine the characteristic of electronic devices. This small discretized distribution can be accurately modeled with an atomistic Kinetic Monte Carlo (KMC) description.

Nevertheless, in order to account for the increasing number of physical phenomena involved in the processing of these devices, several models have to be introduced simultaneously. These models include a charge model for extrinsic diffusion, activation and deactivation mechanisms for dopants, including amorphization and Solid Phase Epitaxy Regrowth (SPER), and a correct description of the formation and ripening of extended defects. This work shows the principles as well as examples of such models. Finally, examples of TCAD simulations of devices, including all these models but focusing on different aspects of the simulation, are also shown.

2. Physical models

The non-lattice KMC technique used in this work[1] tracks the point defects, dopants, impurities and point defect paired dopants as particles. These particles are given random jumps at a rate derived from their diffusivities. Interactions between particles are also included, leading to clustering and re-emission from clusters and trapping and detrapping of impurities. Unlike lattice KMC, non-lattice KMC discards the lattice structure, and accounts for all possible microscopic configurations of a given cluster size through a single effective binding energy. The capture volume for a single particle is assumed to be the distance between second neighbors in the silicon lattice. For extended defects the capture volume is the sum of the capture volumes for the constituent particles.

2.1 Diffusion: The Kick out mechanism

The migration frequency for mobile particles is computed as $\nu = \nu_0 \exp(-E_m / k_B T)$, where υ_0 and E_m are the input parameters that give the microscopic diffusivity for each mobile particle. The acceptor and donor impurities usually diffuse in silicon via pairing with an interstitial or a vacancy[2] while other impurities, like Fluorine, may diffuse without the aid of an extra I or V. The paired dopant point defects break up and re-emit the trapped I or V, becoming substitutional again. The break up frequency equals $\nu = \nu_0 \exp(-E_{bk} / k_B T)$, being E_{bk} is the activation energy for the break up. This energy is modeled as the binding energy plus the migration energy of the emitted particle.

2.2. Activation/deactivation of dopants

Dopants are inactive under certain conditions. These conditions include high dopant concentrations[3] and/or high interstitial or vacancy concentrations[4]. These phenomena can be explained by the clustering of dopant atoms with interstitials or vacancies, and also by dopant precipitation and direct deactivation[5].

2.2.1 Clustering

Impurity clusters are modeled as irregular agglomerations of impurities with vacancies. These clusters can trap new impurities and new interstitials or vacancies. The trapping probabilities are computed as $P_{capture} = \exp(-E_{capture} / k_B T)$, where $E_{capture}$ is the sum of an optional barrier energy plus the absolute value of the binding energy of the trapped particle to the final cluster. These binding energies are computed as the subtraction of the potential energies of final minus initial cluster sizes. The final state depends on the trapped particle. The potential energies are input parameters. Impurity clusters can shrink emitting particles. The emission frequency is given by:

$\nu_{emission} = \nu_0 \exp(-E_{emission} / k_B T)$.

The emission energies are computed as the binding energy of the cluster if the binding is positive, plus the migration energy of the emitted particle and an optional barrier.

2.2.2 Direct deactivation

There is a direct deactivation model available for dopants that deactivate without visible diffusion[5]. This is modeled allowing the substitutional dopants to interact with impurity clusters or with other dopants right after their inclusion in the simulation. Because substitutional dopants do not migrate, these reactions are only possible when two dopants are close enough to each other. The higher the dopant concentration, the higher is this possibility. With high concentrations, the number of dopants close to each other is not negligible, and substitutional dopants will react with others forming clusters and deactivating without diffusion.

2.3. Extended defects

Our model assumes an irregular shape for interstitial clusters with a size less than a given threshold. For bigger sizes, we rearrange them into the {311} defects and/or faulted dislocation loops[6], according to the crystalline geometry data. We assume that irregular clusters retain captured point defects at their original positions. This assumption leads naturally to a roughly spherical size. On the other hand, {311} defects are modeled as parallel strips of interstitials, lying on one of the twelve orientations of a {311} plane. Finally, when a {311} reaches a threshold size that depends on temperature following an Arrhenius plot, it is rearranged into a dislocation loop (DL). In our simulator, DLs are always unfaulted discs lying on a {111} plane.

Extended defects emit their constituent particles. The activation energy for I emission from an I extended defect of size n is calculated as the sum of the I binding energy and migration energy. The emission prefactor is assumed to be proportional to the cluster surface, corresponding to the capture process. The I binding energy for each cluster size is an input parameters, and can be taken directly from existing literature[7, 8]

2.4. Amorphization/recrystallization

Sentaurus KMC gets the coordinates of all the particles for each collision cascade from a Monte Carlo implant simulator[9]. Instead of undergoing immediate recrystallization, point defects are assumed to generate disordered regions, called Amorphous Pockets (APs). The AP activation energy for the recombination of an internal IV pair is related to the number of contained IV pairs. After recombining all its IV pairs, an AP can only dissolve emitting Is or Vs, as a small extended defect. Overlapping APs can give rise to locally amorphized regions and, finally, to a continuum amorphous layer. A SPER process is also implemented converting amorphous boxes back to crystalline silicon with a thermally activated velocity. This process cleans all the damage in the previously amorphized region, but leaves it at the amorphous crystalline interface. Later, this damage will form the end of range defects (EOR), simulated as {311}s and DLs.

2.5. Charge model

In our simulation scheme, particles and defects are treated atomistically, whereas carrier concentrations are treated in a continuum fashion. Charge reactions are much faster than structural reactions and, consequently, we assume electrical equilibrium and a well defined Fermi level, even in situations in which particle concentrations are far from equilibrium.

2.5.1 Concentrations and diffusivities

In our model, each charge state X^j has a different diffusivity. The relative concentrations are[10]

$$\frac{[X^{j}]}{[X^{j+1}]} = \exp\left(\frac{e_F - e(j+1, j)}{k_B T}\right)$$

Where we denote by e(j+1,j) the energy level associated with the charge transitions between X^{j+1} and X^j. We assume the same degeneracy factor for each state. The concentrations of charged point defects are controlled by the charged transitions. Therefore, the formation energy or a charged defect can be obtained from the formation energy for the neutral particle, and the Fermi level (e_F), using

$E_f(X^{j+1}) = E_f(X^j) + e_F - e(j+1, j)$.

In the absence of an electric field each charge state has a jump frequency that does not depend on e_F. An electric field ξ introduces a gradient into the formation energy of a charged particle, inducing an asymmetry in the jump probabilities in both positive and negative directions:

$\frac{\upsilon^+}{\upsilon^-} = \exp\left(\frac{jq\lambda\xi}{k_B T}\right)$, being q the electron charge.

The charge model also affects the interaction between particles. Reactions between particles with the same sign are forbidden to account for the electrostatic repulsion. It is only necessary to specify the binding energies between the neutral interstitials or vacancies (X) and the charged substitutional dopants (A) so that the binding energies of the rest of the charge states are computed using microscopic reversibility links as:

$E_b\left(AX^j\right) = E_b(AX^j) + e_{AX}(j+1, j) - e_X(j+1-k, j-k)$.

2.5.2 Implementation

As we have already mentioned, our model assumes that the electronic transitions are much faster than the atomic diffusion and reactions; it implies the necessity of implement charge update mechanisms. In particular, three of these mechanisms have been implemented[11] to maintain an accurate description of the electronic state of the dopants.

- Global update. Periodical review and update of all the particles. The probability for a particle to be in a particular charge state is computed as: $P^j = \frac{[X^j]}{\sum_j [X^j]}$
- Charge update for the mobile particles. This update is performed for any mobile particle each time it moves. In this case, to avoid artifacts in the simulation, it is necessary to assign a probability that also depends on its migration frequency: $P^j = \frac{P^j \nu_m(X^j)}{\sum_j P^j \nu_m(X^j)}$

- Charge update for pairing and break-up reactions. This algorithm ensures that the right concentrations of species are not disturbed by the pairing and break up of dopants. The probability used is very similar to the previous one, except for the use of the break up frequency instead of the migration frequency.

To compute the electron concentration, and then the Fermi level, the simulation domain is divided into a tensor product where each element is a small 3D rectangle. These elements can be as small as 1 nm^3. The algorithm does not only count the number of active dopants for each element (other charged particles are supposed to give a negligible contribution), but also averages several elements, smoothing out the electron concentration over the elements contained in a sphere whose radius is the Debye length. This smoothing is extremely important to avoid artificial high concentrations due to the discrete nature of the particles and the small volume of the internal elements[11].

3. Simulation examples

A validation of the models explained in this work, especially the charge model, can be seen in figure 1. It shows the dopant redistribution in a pn junction. An initially uniform $1x10^{18}$ cm^{-3} B concentration is implanted with $2x10^{15}$ cm^{-2}, 50keV As and annealed for 2 hours. The boron pile up is due to the different B diffusivity in the n region. The excellent agreement with the experimental results[12] confirms the right implementation of the diffusion, impurity cluster and charge model as well as the accuracy of the initial dopant and point defect distribution given by the MC implant code.

Figures 2a and 2b correspond to comparisons between experimental results and our atomistic simulator. Fig. 2a shows SIMS profiles[4] of $4.5x10^{19}$ B spikes after 40 keV $9x10^{13}$ cm^{-2} Si implant and 5, 50, 500 and 2100 s anneal at 800 ^oC. The peak corresponds to immobile boron interstitial clusters, formed in a zone rich in both Si interstitials and boron, while the Gaussian-like profile

shows the electrically active boron diffusion. In contrast, Fig. 2b shows the deactivation of As in conditions of thermally generated intrinsic point defects[13]. The structure consists of a buried B layer and an initially fully activated implanted and laser-melt annealed superficial As layer. After 8 min at 750 ^{o}C the boron has largely diffused. This is due to the interstitial injection during the rapid deactivation of arsenic. The high concentration of As leads to the formation of some As_4 clusters. These clusters are unstable and emit I transforming into As_4V. This I supersaturation creates the transient enhanced diffusion of the boron marker. Lines: Sentaurus KMC. Symbols: Experiment[14].

Figure 3 indicates the validity of the extended defect model explained in this work. It shows the comparison between the experimental I supersaturation reported by Ref [7], and the results of our simulations. Agreement is only achieved when the I clusters are allowed to ripen with different energies, one for each size.

Figure 4 shows the recrystallization of an amorphous layer under the source of a FET transistor. The evolution of the recrystallization front in time cleans up the damage created during the implant. At the end, the only remaining damage is located close to the amorphous/crystalline (A/C) interface. These defects will later create EOR defects.

Figure 5 shows a whole MOSFET, with a gate length of 30nm, entirely simulated using the KMC models explained in this work. All the models described have to be active in order to correctly simulate devices like this one. The top picture shows the doping concentration at the end of the simulation. The bottom one shows the particles and defects as simulated. In this case, the thermal budget is not enough to dissolve the extended defects: there are {311}s under the source and the drain. These {311}s are the remnants of the damage accumulated at the A/C interface after SPER.

Finally, figure 6 shows the importance of 3D atomistic simulations to account for geometrical effects. These effects are more important as the dimensions of the devices become ever shorter. The same implant and subsequent diffusion has been performed in 70x70nm^2 and 170x170nm^2 devices surrounded by silicon trench isolation (STI). While the small layout contains no defects, the bigger is still rich in {311} and DLs for the same implant and subsequent annealing. The STI creates an extra interface that acts as a sink for interstitial. The distance between extended defects and the interface plays a very important role for the growth of extended defects in 1D structures, but this effect is even more important for 2 and 3D layouts.

4. Conclusions

In conclusion, we have developed physically-based atomistic models that explain and predict the majority of mechanisms involved in the processing of Silicon for microelectronics. These models include the intrinsic and extrinsic diffusion of dopants, their activation and deactivation forming impurity clusters, a damage accumulation, amorphization and SPER model, and the formation of extended defects that control the transient enhanced diffusion. Simulation examples of these different models have also been shown. Finally, we have shown how these different models, once integrated and working at the same time in a kinetic Monte Carlo simulator, are able to successfully simulate deep-submicron devices. The simulator can be also used to account for the study and prediction of 2 and 3 dimensional effects.

5. Acknowledgments

Many thanks to Minna Vallentine, at Mountain View/Los Altos Adult School, for proof-reading this paper.

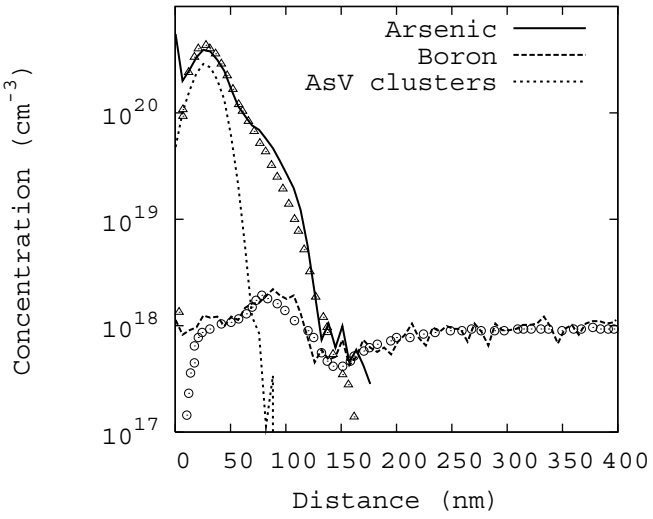
Arsenic
Boron
AsV clusters
Concentration (cm-3)
10^20
10^19
10^18
10^17
0 50 100 150 200 250 300 350 400
Distance (nm)

Figure 1.

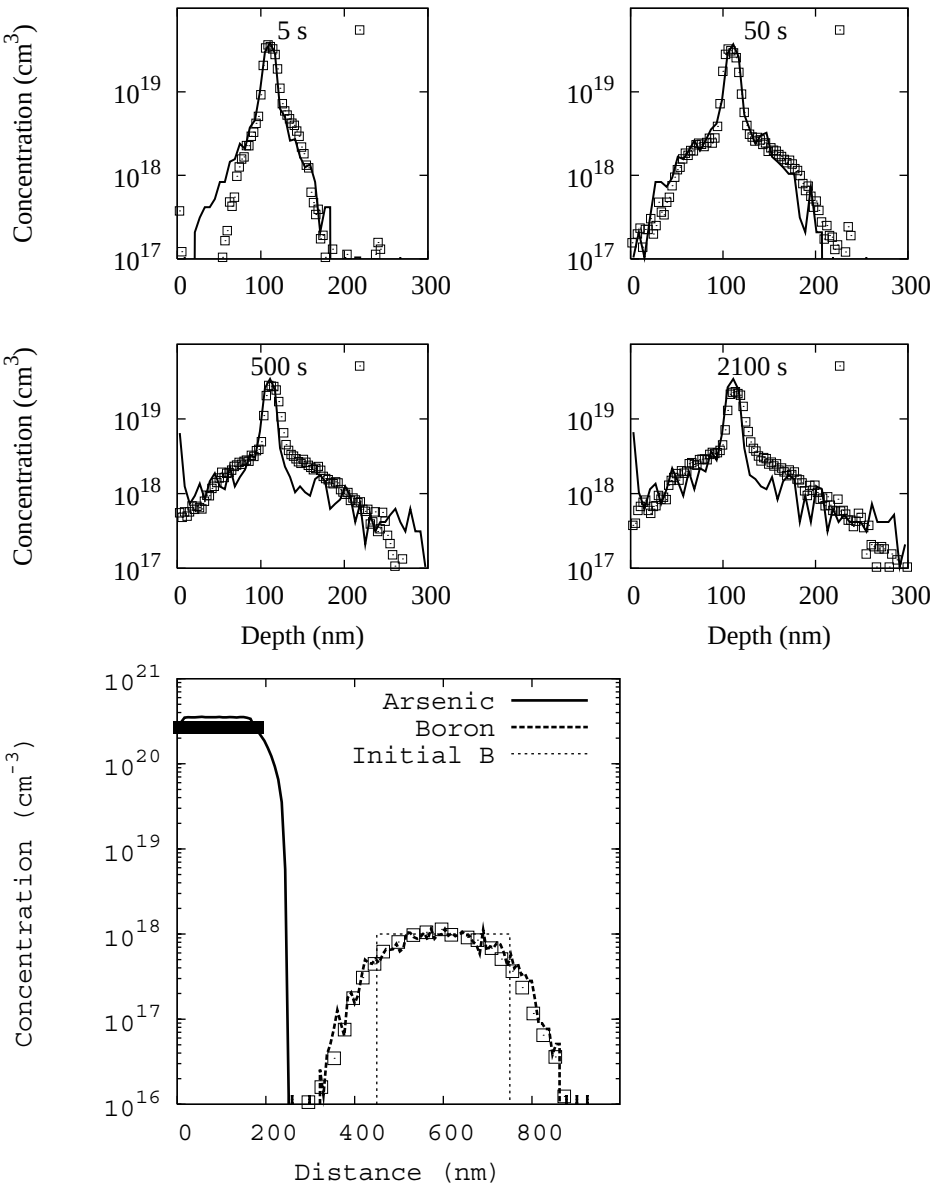
5 s
50 s
500 s
2100 s
Concentration (cm3)
Depth (nm)
Arsenic
Boron
Initial B
Concentration (cm-3)
Distance (nm)

Fig 2a and 2b.

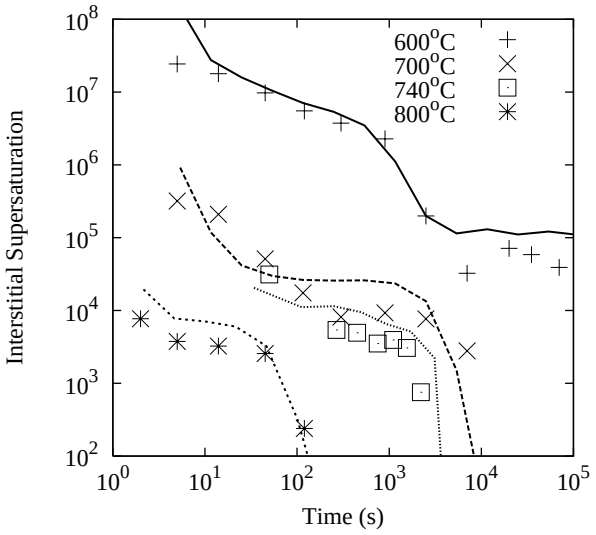
Interstitial Supersaturation
Time (s)
600°C
700°C
740°C
800°C
10^8
10^7
10^6
10^5
10^4
10^3
10^2
10^0
10^1
10^2
10^3
10^4
10^5

Figure 3.

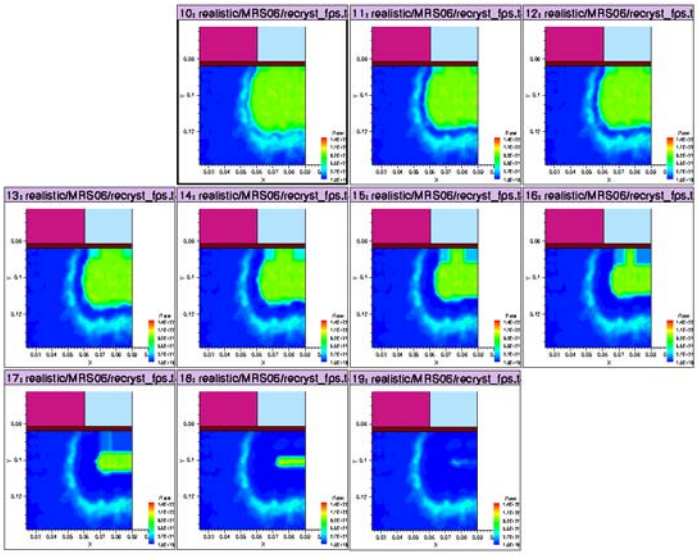

Figure 4.

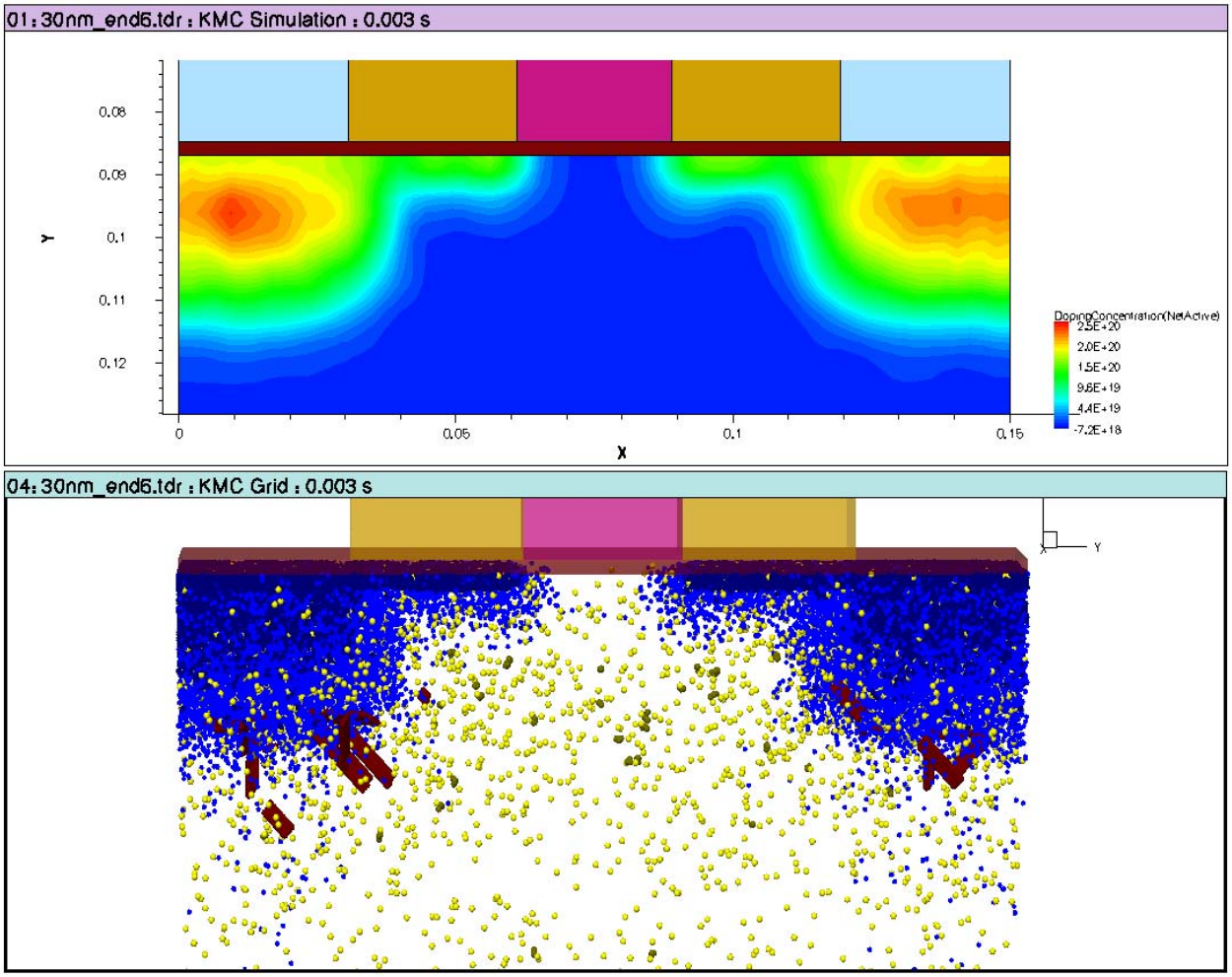
01: 30nm_end6.tdr : KMC Simulation : 0.003 s
0.08
0.09
0.1
0.11
0.12
Y
0
0.05
0.1
0.15
X
DopingConcentration(NetActive)
2.5E+20
2.0E+20
1.5E+20
9.6E+19
4.4E+19
-7.2E+18
04: 30nm_end6.tdr : KMC Grid : 0.003 s
X
Y

Figure 5.

a)

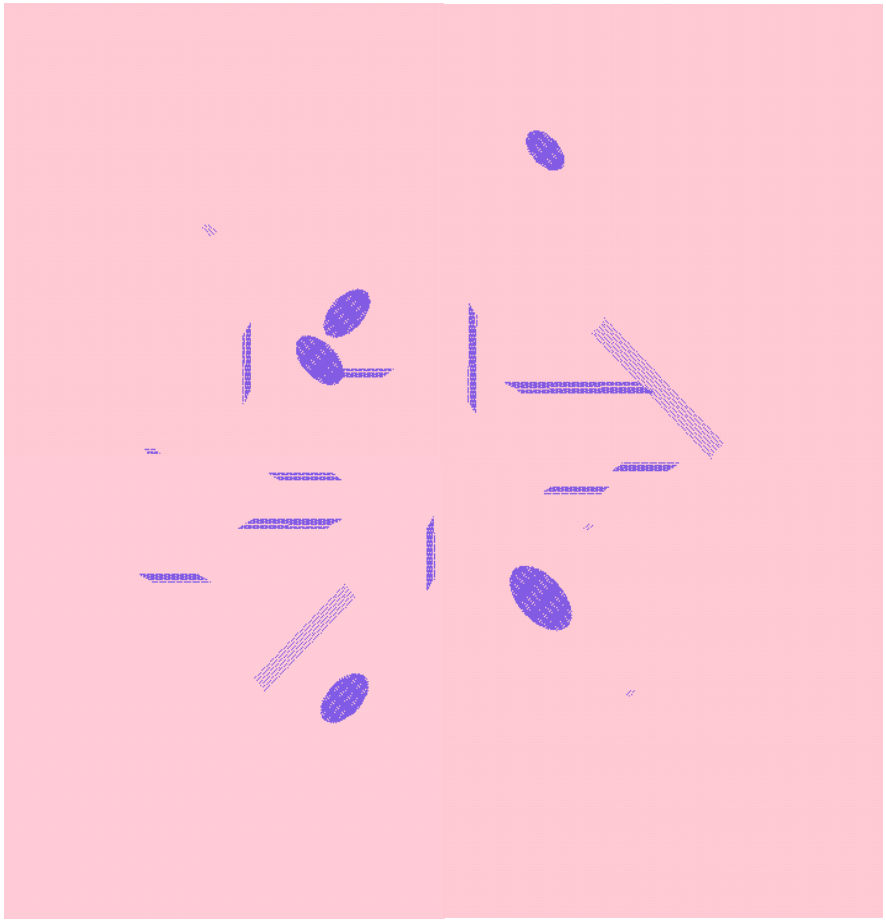

b)

Figure 6.

FIGURE CAPTIONS

Fig 1. Boron pile-up in a pn junction. An initial boron background concentration ($1x10^{18}$ cm^{-3}) has been implanted with As, 50 keV, $2x10^{15}$ cm^{-2} and annealed for 2h at 750 ^{o}C. Symbols : Experimental results from Ref. 12. Lines. Sentaurus KMC simulations. The electronic concentration, is also represented. The difference between the arsenic profile and the electronic concentration is due to the presence of AsV clusters.

Fig 2. B and As impurity clusters. a)Simulated (lines) and experimental (symbols) profiles of a $4.5x10^{19}$ cm^{-3} B spike after a Si into Si implant, 40keV, $9x10^{13}$ cm^{-2} and 5, 50, 500 and 2100 s annealing at 800 ^{o}C. Experimental data taken from Ref. 4. b) Buried B layer and laser-melt As layer after 8 minutes at 750 ^{o}C. Symbols : Experimental data taken from Ref. 14. Lines : Sentaurus KMC simulation.

Fig. 3. Interstitial supersaturation as a function of time for different annealing temperatures. 600, 700 and 800 ^{o}C after a 40keV $2x10^{13}$ cm-^{2} and 740 ^{o}C, after a 40 keV, $6x10^{13}$ cm^{-2} implant. Symbols : experimental values[7] scaled to give the same DC product as the simulation. Lines: Sentaurus KMC results.

Fig 4. Gate and source of a FET during the time evolution of the SPER after a Ge preamorphizing implant. The SPER cleans all the defects, leaving only a high damaged region close to the original A/C interface. These defects will form EOR defects.

Fig 5. Top. 2D projection of the active dopant concentration in the source, gate and drain of a small MOSFET (gate length is 30nm) at the end of all the processing steps. Bottom. Atomistic view of the same transistor. It should be noticed the presence of {311}. Light yellow: Active boron. Dark yellow: BICs. Red: Interstitials in {311}. Light blue : Active Arsenic. Dark blue: Arsenic in clusters.

Fig 6. a) Top view of a 70x70 nm^{2} simulation, surrounded by STI, after a 30keV, $5x10^{14}$ cm^{-2} Ge implant and a 950 ^{o}C spike annealing. b) Same simulation than before, but with a 140x140 nm^{2} area. The smaller the distance to the STI interface the easier to anneal the extended defects.

REFERENCES

[1] M. Jaraiz, P. Castrillo, R. Pinacho, I. Martin-Bragado, and J. Barbolla, in Simulation of Semiconductor Processes and Devices 2001, pp. 10-17.

[2] P. M. Fahey, P. B. Griffin and J. D. Plummer. “Point Defects and Dopant Diffusion in Silicon”. Rev. Mod. Phys. Vol 61, pp. 289-384, 1989.

[3] P.A. Stolk, H.J. Gossmann, D.J. Eaglesham, D.C. Jacobson, J.M. Poate and H.S. Luftman. Appl. Phys. Lett., vol. 66, p. 568. 1995

[4] L. Pelaz, M. Jaraiz, G.H. Gilmer, H.J. Gossman, C.S. Rafferty, D.J. Eaglesham and J.M. Poate. App. Phys. Lett., vol. 70, pp. 2285-2287, 1997.

[5] D.C. Muller. Ph.D. Thesis. Series in Microelectronics, vol. 151, Ed. Hartung-Gorre Verlag Konstanz, 2004

[6] Ignacio Martin-Bragado. Ph.D. Thesis. Universidad de Valladolid, Valladolid, Spain, 2005.

[7] N.E.B. Cowern, G. Manino, P.A. Stolk, F. Roozeboom, H.G.A. Huizing, J.G.M. van Berkum, F. Cristiano, A. Claverie and M. Jaraiz. Phys. Rev. Lett. 82(22) 4460-4463

[8] F. Cristiano, J. Grisiola, B. Colombeau, M. Omri, B. de Mauduit, A. Claverie, L.F. Giles and N.E.B. Cowern. J. Appl. Phys. 87, 8420 (2000)

[9] S. Tian. J. App. Phys., vol 93. no. 10, pp. 5893-5904, 2003.

[10] I. Martin-Bragado, M. Jaraiz, P. Castrillo, R. Pinacho and J. Barbolla. Phys. Rev. B. Vol 72, pp. 035202. 2005.

[11] I. Martin-Bragado, P. Castrillo, M. Jaraiz, R. Pinacho, J.E. Rubio, J. Barbolla and V. Moroz. J. App. Phys., 98, 053709

[12] H.S. Chao, P.B. Griffin and J.D. Plummer. Mat. Res. Soc. Symp. Proc. Vol. 469, pp 347-352. 1997.

[13] R. Pinacho, M. Jaraiz, P. Castrillo, I. Martin-Bragado, J.E. Rubio and J. Barbolla. Appl. Phys. Lett. 86. 252103 (2005).

[14] P.M. Rousseau, P.B. Griffin, W.T. Fang and J.D. Plummer. J. Appl. Phys. 84(7) 3593